

Approximate message-passing with spatially coupled structured operators, with applications to compressed sensing and sparse superposition codes

Jean Barbier[†], Christophe Schülke^{U,∩} and Florent Krzakala^{†,★}

[†] Laboratoire de Physique Statistique, CNRS UMR 8550, Ecole Normale Supérieure & Université Pierre et Marie Curie, 24 rue Lhomond, 75231 Paris, France

[★] Sorbonne Universités, UPMC Université Paris 06, UMR 8550 75231, Paris, France

^U Université Paris Diderot, Sorbonne Paris Cité, 75205 Paris, France

[∩] Dipartimento di Fisica, Sapienza Università di Roma, p.le A. Moro 2, 00185 Rome, Italy

E-mail: jean.barbier@ens.fr, christophe.schulke@espci.fr, florent.krzakala@ens.fr

Abstract. We study the behavior of Approximate Message-Passing, a solver for linear sparse estimation problems such as compressed sensing, when the i.i.d matrices—for which it has been specifically designed—are replaced by structured operators, such as Fourier and Hadamard ones. We show empirically that after proper randomization, the structure of the operators does not significantly affect the performances of the solver. Furthermore, for some specially designed spatially coupled operators, this allows a computationally fast and memory efficient reconstruction in compressed sensing up to the information-theoretical limit. We also show how this approach can be applied to sparse superposition codes, allowing the Approximate Message-Passing decoder to perform at large rates for moderate block length.

Sparse reconstruction problems have recently witnessed a burst of activity in a wide range of applications spanning from signal processing [1] to coding theory [2]. In particular, compressed sensing (CS) techniques [1, 3] have suggested entirely new ways of capturing signals and images, such as in the single-pixel camera [4].

The physics community became interested in these topics due to the link with spin glass physics, as it has been the case with constraint satisfaction problems [5–7] (and actually, compressed sensing itself can also be seen as a finite temperature constraint satisfaction problem). For instance, the compressed sensing problem can be interpreted as a densely connected (i.e. with infinite range interactions) spin glass model of continuous spins in an external field, where the interactions enforce the state of the spins to verify the linear measurements (up to noise, interpreted as the temperature) and the external field would be the prior in the Bayesian setting. The problem of inferring the minimum mean-squared error (MMSE) signal that generated the measurements (or “planted” solution in the physics language) is equivalent to sampling from the Boltzmann measure of the appropriate spin glass model, and the maximum-a-posteriori (MAP) estimate is given by the ground state of the Hamiltonian ([8, 9] for a more detailed discussion of the links between compressed sensing and spin glass physics). Similar mappings can be established for many other computer science, inference and machine learning problems [10]. The typical phenomenology of spin glasses is observed in these inference problems: phase transitions and dynamical slowing down of the reconstruction algorithms near the critical “temperature” (the critical measurement rate in CS). Furthermore, message-passing algorithms, such as belief-propagation, can be interpreted in terms of the cavity method written for single instances, although the cavity method has been originally developed for computing thermodynamical quantities (i.e. averaged over the source of disorder) in spin glasses [6].

The aim of this paper is to study one way to tackle very large single instances of inference problems such as compressed sensing. To work with large signals and matrices, however, one needs fast and memory efficient solvers. Indeed, the mere storage of the measurement matrix in memory can be problematic as soon as the signal size $N > O(10^4)$. A classical trick (see for instance [11]) is thus to replace the random sensing matrix with a structured one, typically random modes of a Fourier or Fourier-like matrix. The use of the fast Fourier transform makes matrix multiplication faster ($O(N \log N)$ instead of $O(N^2)$ operations), and thus both speeds up the reconstruction algorithm and removes the need to store the matrix in memory. This is also important for coding applications where $O(N^2)$ operations can be burdensome for the processor.

Although CS reconstruction is typically based on convex optimization [12], we shall consider here an alternative technique, the Approximate Message-Passing (AMP) algorithm, that allows Bayesian reconstruction [8, 12–15] with much improved performances. Of special interest has been the joint use of AMP and specially designed [8] random matrices based on spatial-coupling [16–18]: this has been shown to achieve optimal information-theoretic performance in such sparse estimation problems [8, 19].

Let us summarize the contributions of the present paper: while using Fourier or

Hadamard matrices has often been done with AMP (see e.g. [20, 21]), we provide here a close examination of the performance of AMP with Fourier and Hadamard operators for complex and real sparse signals respectively. As suggested by the heuristic replica analysis [22, 23], such matrices often lead to better performances than random ones.

Secondly, inspired by the Gabor construction of [20] —that allowed optimal sampling of a random signal with sparse support in frequency domain— we extend the construction of spatially coupled (or “seeded” [8, 9]) matrices to a structured form using fast Fourier/Hadamard operators, which allow to deal with large signal sizes. Given the lack of theoretical guaranties, we numerically study this strategy on synthetic problems, and compare its performance and behavior with those obtained with random i.i.d Gaussian matrices. Our main result is that after some randomization procedure, structured operators appear to be nearly as efficient as random i.i.d matrices. In fact, our empirical performances are as good as those reported in [8, 9] despite the drastic improvement in computational time and memory.

Finally, to show the potential of these operators, we apply them to sparse superposition codes, an error-correcting scheme for the Gaussian Channel [2, 24, 25] for which an AMP decoder has recently been proposed [26]. We will show empirically that the use of the spatially coupled Hadamard operator allows to get closer to the capacity with the AMP decoder, even for moderate block-lengths.

1. Problem setting

In the following, complex variables will be underlined: $\underline{x}_j = x_{j,1} + ix_{j,2} \in \mathbb{C}$, bold letters will be used for vectors and capital bold letters for matrices/operators. We will write $x \sim \mathcal{N}_{\bar{x}, \sigma^2}$ if x is a Gaussian random variable with mean \bar{x} and variance σ^2 , and $\underline{x} \sim \mathcal{CN}_{\bar{x}, \sigma^2}$ if the real and imaginary parts x_1 and x_2 of the random variable \underline{x} are independent and verify $x_1 \sim \mathcal{N}_{\Re \bar{x}, \sigma^2}$ and $x_2 \sim \mathcal{N}_{\Im \bar{x}, \sigma^2}$. $\delta(\cdot)$ is the Dirac delta function and $\delta_{i,j}$ is the Kronecker symbol.

The generic problem we consider is as follows: An unknown signal $\underline{\mathbf{x}} = [\underline{x}_1, \dots, \underline{x}_N]$ is passed through a linear $M \times N$ operator $\underline{\mathbf{F}} = \{\underline{F}_{\mu i}\}$, giving $\underline{\tilde{\mathbf{y}}} = [\tilde{y}_1, \dots, \tilde{y}_M]$ such that:

$$\tilde{y}_\mu = \sum_{i=1}^N \underline{F}_{\mu i} \underline{x}_i. \quad (1)$$

In the most general setting, a noisy version $\underline{\mathbf{y}} = [y_1, \dots, y_M]$ of $\underline{\tilde{\mathbf{y}}}$ is then measured:

$$\underline{\mathbf{y}} = \underline{\tilde{\mathbf{y}}} + \underline{\boldsymbol{\xi}}, \quad \underline{\boldsymbol{\xi}} = [\underline{\xi}_1, \dots, \underline{\xi}_M], \quad (2)$$

with $\underline{\xi}_\mu \sim \mathcal{CN}_{0, \Delta} \forall \mu \in \{1, \dots, M\}$. The goal is to recover the original vector from the noisy measurements.

We shall consider two particular settings of this problem in the present paper. The first one is noiseless compressed sensing with real and complex variables. We will use the

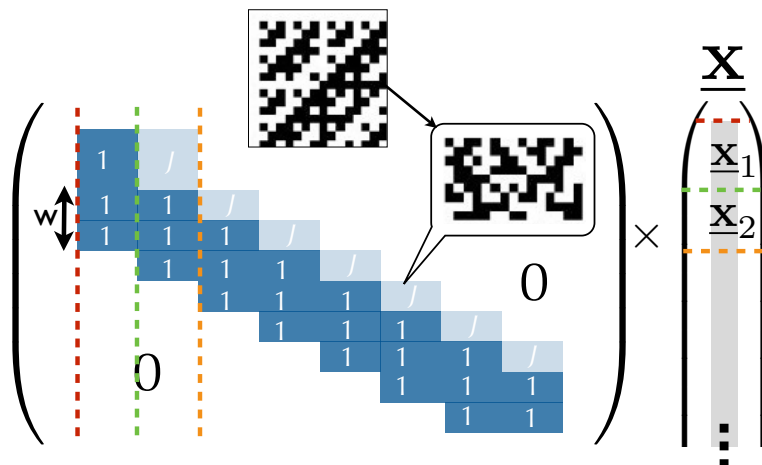


Figure 1. Representation of the spatially coupled Hadamard sensing matrix used in our study. The operator is decomposed in $L_r \times L_c$ blocks, each being made of N/L_c columns and $\alpha_{\text{seed}}N/L_c$ lines for the blocks of the first block-row, $\alpha_{\text{rest}}N/L_c$ lines for the following block-rows (these follow from the definition of $\alpha := M/N$ combined with (4)), with $\alpha_{\text{seed}} > \alpha_{\text{rest}}$. The figure shows how the lines of the original Hadamard matrix (of size $N/L_c \times N/L_c$) are randomly selected, re-ordered and sign-flipped to form a given block of the final operator. There is a number w (the coupling window) of lower diagonal blocks with elements $\in \{\pm 1\}$ as the diagonal blocks, the upper diagonal blocks have elements $\in \{\pm\sqrt{J}\}$ where \sqrt{J} is the coupling strength, all the other blocks contain only zeros. The colored dotted lines help to visualize the block decomposition of the signal induced by the operator structure: each block of the signal will be reconstructed at different times in the algorithm (see Fig. 4 main figure). The procedure is exactly the same for constructing spatially-coupled Fourier operators, replacing the small Hadamard operator from which we construct the blocks by a small Fourier operator. The parameters that define the spatially coupled operator ensemble $(L_c, L_r, w, \sqrt{J}, \alpha_{\text{seed}}, \alpha_{\text{rest}})$ remain the same.

following Gauss-Bernoulli distribution to generate ρ -sparse complex random vectors:

$$P(\underline{\mathbf{x}}) = \prod_{j=1}^N [(1 - \rho)\delta(\underline{x}_j) + \rho \mathcal{CN}_{\bar{x}, \sigma^2}(\underline{x}_j)]. \quad (3)$$

Here we shall assume that the correct values for ρ , \bar{x} , σ^2 and Δ , as well as the empirical signal distribution (3) are known. As shown empirically in [8, 9, 15] these parameters can be learned efficiently with an expectation maximization procedure if unknown. A remarkable result is that if $\underline{\mathbf{x}}$ is sparse, i.e. has a fraction $(1 - \rho)$ of strictly zero components, then it is possible to recover $\underline{\mathbf{x}}$ from the knowledge of $\underline{\mathbf{y}}$ and $\underline{\mathbf{F}}$ even if the system is underdetermined, i.e. the measurement rate $\alpha := M/N < 1$. An information-theoretical lower bound for the measurement rate is $\alpha_{\text{min}}(\rho) = \rho$: no algorithm can perform a reconstruction below this bound. CS algorithms do not usually reach this bound, but are characterized by a phase transition that depends on the sparsity and the noise levels $\alpha_{\text{PT}}(\rho, \Delta) > \rho$, above (below) which the algorithm succeeds (fails) with high probability (i.e. that tends to one as the signal size $N \rightarrow \infty$).

In the last part of the paper, we will consider sparse superposition codes. In that

case, we will denote the length of vector \mathbf{x} as L and each of its components will be a B -dimensional real variable. The prior, for this problem, will enforce the condition that each of the B -dimensional variables is pointing towards one of the summits of the B -dimensional hypercube, i.e. only one component among the B is 1, the others are 0. Such codes are, in a proper limit, capacity achieving [2]. However, in the standard version of the problem, AMP decoding is limited to a region far from capacity [26]. We will come back to this problem in section 3 and will first concentrate on noiseless compressed sensing.

1.1. Spatially coupled measurement matrices

AMP is a CS solver that can perform Bayes-optimal inference, and the position of its phase transition $\alpha_{\text{AMP}}(\rho)$ can be determined exactly in the $N \rightarrow \infty$ limit by State Evolution (SE) analysis [27]. Though it was initially designed for i.i.d random matrices, it was recently empirically shown, through the use of the replica method [9], and then, also, theoretically proven [19] that the use of spatially coupled matrices allows to lower the phase transition from $\alpha_{\text{AMP}}(\rho) > \rho$ to $\alpha_{\text{min}}(\rho) = \rho$.

Fig.1 shows such a spatially coupled matrix: It has a block structure with $L_r \times L_c$ blocks, each block containing either only zeros or a different random selection of modes of a Fourier or Hadamard operator. Each of these blocks is constructed from the same original operator of size $N/L_c \times N/L_c$ and the differences from one block to another arise from the selected modes, their permutation and signs that are randomly changed. One of the blocks is called the seed (usually the block on the upper left corner as shown on Fig. 1) and its ratio of number of lines over number of columns α_{seed} has to be larger than $\alpha_{\text{AMP}}(\rho)$ for the spatial coupling to work. All the other blocks can have their α_{rest} asymptotically as low as ρ . The first block of the signal is then easily reconstructed due to its high α_{seed} , and the solution spreads through the entire signal thanks to the coupling introduced by the non-diagonal blocks. This “nucleation” effect (that has the same phenomenology than the surfusion of super-cooled water for example) is discussed in full details in [9, 16].

The link between the overall measurement rate α , that of the seed α_{seed} and that of the bulk α_{rest} is given by:

$$\alpha_{\text{rest}} = \frac{\alpha L_c - \alpha_{\text{seed}}}{L_r - 1} = \alpha \frac{L_c - \beta_{\text{seed}}}{L_r - 1}. \quad (4)$$

In practice, α is fixed and $\alpha_{\text{seed}} := \alpha \beta_{\text{seed}}$ as well by fixing β_{seed} . α_{rest} is then deduced from (4). In the rest of the paper, we will define the spatially coupled ensemble by $(L_c, L_r, w, \sqrt{J}, \alpha, \beta_{\text{seed}})$ instead of $(L_c, L_r, w, \sqrt{J}, \alpha_{\text{seed}}, \alpha_{\text{rest}})$.

1.2. The AMP algorithm

We now describe the AMP algorithm for complex signals (cancelling all the imaginary parts, AMP for real signals is recovered). AMP is an iterative algorithm that calculates successive estimates of $\underline{\mathbf{x}}$ and $\underline{\tilde{\mathbf{y}}}$, as well as uncertainties on those estimates. It uses

both linear steps, involving matrix multiplications, and non-linear steps, involving thresholding functions \underline{f}_{a_i} and f_{c_i} (the underline means that \underline{f}_{a_i} outputs a complex number). These are either calculated from the actual signal distribution $P(\underline{\mathbf{x}})$, in which case the algorithm is Bayes-optimal, or from a sparsity-inducing Laplace prior, in which case AMP solves an L_1 minimization problem.

In order to avoid confusion with the literature where variations of AMP are already presented, we will refer to the Bayes-optimal AMP by ‘‘BP’’ and ‘‘c-BP’’ for the real and the complex case respectively, and to the L_1 -minimizing version by ‘‘LASSO’’ and ‘‘c-LASSO’’ respectively (where BP stands for Belief Propagation, of which AMP is an adaptation). As the thresholding functions are applied componentwise, the time-consuming part of the algorithm is the matrix multiplications in the linear step. Here, we use Fourier and Hadamard operators in order to reduce the complexity of the matrix multiplications from $O(N^2)$ to $O(N \log N)$. The authors of [20] have used a related, yet different way to create spatially coupled matrices using a set of Gabor transforms.

We define \mathbf{e}_c , with $c \in \{1, \dots, L_c\}$, a vector of size $N_c = N/L_c$, as the c^{th} block of \mathbf{e} (of size N) and \mathbf{f}_r , with $r \in \{1, \dots, L_r\}$, a vector of size $N_r = \alpha_r N/L_c$ as the r^{th} block of \mathbf{f} (of size M). For example, in Fig. 1, the signal $\underline{\mathbf{x}}$ is decomposed as $[\underline{\mathbf{x}}_1, \dots, \underline{\mathbf{x}}_{L_c}]$. The notation $\{i \in c\}$ (resp. $\{\mu \in r\}$) means all the components of \mathbf{e} that are in the c^{th} block of \mathbf{e} (resp. all the components of \mathbf{f} that are in the r^{th} block of \mathbf{f}). The algorithm requires four different operators performing the following operations:

$$\begin{aligned} \tilde{O}_\mu(\mathbf{e}_c) &:= \sum_{\{i \in c\}}^{N/L_c} |\underline{F}_{\mu i}|^2 e_i, & O_\mu(\mathbf{e}_c) &:= \sum_{\{i \in c\}}^{N/L_c} \underline{F}_{\mu i} e_i, \\ \tilde{O}_i(\mathbf{f}_r) &:= \sum_{\{\mu \in r\}}^{\alpha_r N/L_c} |\underline{F}_{\mu i}|^2 f_\mu, & O_i^*(\mathbf{f}_r) &:= \sum_{\{\mu \in r\}}^{\alpha_r N/L_c} \underline{F}_{\mu i}^* f_\mu. \end{aligned}$$

α_r is the measurement rate of all the blocks at the r^{th} block-row, for example in Fig. 1, $\alpha_1 = \alpha_{\text{seed}}$ and $\alpha_j = \alpha_{\text{rest}} \forall j > 1$ and $F_{\mu i}^*$ is the complex conjugate of $F_{\mu i}$. Because the value of $|\underline{F}_{\mu i}|^2$ is either 0, 1 or $J \forall (\mu, i)$ as we use Hadamard or Fourier operators (it can be read on Fig. 1), all these operators do not require matrix multiplications as they are implemented as fast transforms ($O_\mu()$ and $O_i^*()$) or simple sums ($\tilde{O}_\mu()$ and $\tilde{O}_i()$). It results in the updates for AMP [28], with a generic operator, see Fig. 2.

Here, we give the functions \underline{f}_{a_i} and f_{c_i} that are calculated from $P(\underline{\mathbf{x}})$ and are thus Bayes-optimal, which is not the case for LASSO and c-LASSO [29]. For BP, they are given in [9, 30]. For c-BP, the signal is complex and drawn from the distribution (3), and the thresholding functions (which give posterior scalarwise estimates of the mean and variance) are given by:

$$\begin{aligned} \underline{f}_{a_i}(\Sigma^2, \underline{R}) &= g\rho\chi^2 \underline{M}/Z, \\ f_{c_i}(\Sigma^2, \underline{R}) &= (g\rho\chi^2 (|\underline{M}|^2 + 2\chi^2)/Z - |\underline{f}_a(\Sigma^2, \underline{R})|^2)/2, \end{aligned}$$

with the following definitions:

$$\underline{M} := (\sigma^2 \underline{R} + \Sigma^2 \bar{x})/(\Sigma^2 + \sigma^2), \quad \chi^2 := \Sigma^2 \sigma^2 / (\Sigma^2 + \sigma^2),$$

```

1:  $t \leftarrow 0$ 
2:  $\delta_{\max} \leftarrow \epsilon + 1$ 
3: while  $t < t_{\max}$  and  $\delta_{\max} > \epsilon$  do
4:    $\Theta_{\mu}^{t+1} \leftarrow \sum_{c=1}^{L_c} \tilde{O}_{\mu}(\mathbf{v}_c^t)$ 
5:    $\underline{\mathbf{w}}_{\mu}^{t+1} \leftarrow \sum_{c=1}^{L_c} O_{\mu}(\underline{\mathbf{a}}_c^t) - \Theta_{\mu}^{t+1} \frac{\underline{\mathbf{y}}_{\mu} - \underline{\mathbf{w}}_{\mu}^t}{\Delta + \Theta_{\mu}^t}$ 
6:    $\Sigma_i^{t+1} \leftarrow \left[ \sum_{r=1}^{L_r} \tilde{O}_i([\Delta + \Theta_r^{t+1}]^{-1}) \right]^{-1/2}$ 
7:    $\underline{\mathbf{R}}_i^{t+1} \leftarrow \underline{\mathbf{a}}_i^t + (\Sigma_i^{t+1})^2 \sum_{r=1}^{L_r} O_i^* \left( \frac{\underline{\mathbf{y}}_r - \underline{\mathbf{w}}_r^{t+1}}{\Delta + \Theta_r^{t+1}} \right)$ 
8:    $v_i^{t+1} \leftarrow f_{c_i}((\Sigma_i^{t+1})^2, \underline{\mathbf{R}}_i^{t+1})$ 
9:    $\underline{\mathbf{a}}_i^{t+1} \leftarrow \underline{f}_{a_i}((\Sigma_i^{t+1})^2, \underline{\mathbf{R}}_i^{t+1})$ 
10:   $t \leftarrow t + 1$ 
11:   $\delta_{\max} \leftarrow \max_i (|\underline{\mathbf{a}}_i^t - \underline{\mathbf{a}}_i^{t-1}|^2)$ 
12: end while
13: return  $\{a_i\}$ 

```

Figure 2. The AMP algorithm written with operators. Depending on whether it is used on a real or complex signal, with Bayes-optimal or sparsity-inducing thresholding functions \underline{f}_{a_i} and f_{c_i} , we call it BP, c-BP, LASSO or c-LASSO. ϵ is the accuracy for convergence and t_{\max} the maximum number of iterations. A suitable initialization for the quantities is ($\underline{\mathbf{a}}_i^{t=0} = 0$, $v_i^{t=0} = \rho\sigma^2$, $\underline{\mathbf{w}}_{\mu}^{t=0} = \underline{\mathbf{y}}_{\mu}$). Once the algorithm has converged, i.e. the quantities do not change anymore from iteration to iteration, the estimate of the i^{th} signal component is $\underline{\mathbf{a}}_i^t$. The variable $\underline{\mathbf{w}}$ is an estimate of $\tilde{\mathbf{y}}$, while $\underline{\mathbf{R}}$ and $\underline{\mathbf{a}}$ are estimates of $\underline{\mathbf{x}}$; Θ , Σ and \mathbf{v} are their respective uncertainties. The nonlinear thresholding functions \underline{f}_{a_i} and f_{c_i} take into account the prior distribution $P(\underline{\mathbf{x}})$. In the case of compressed sensing, applying \underline{f}_{a_i} to a $\underline{\mathbf{R}}_i^{t+1}$ close to zero will give a result even closer to zero, while bigger inputs will be left nearly unchanged, thus favoring sparse solutions.

$$g := e^{-\frac{1}{2} \left(\frac{|\bar{x}|^2}{\sigma^2} + \frac{|\underline{\mathbf{R}}|^2}{\Sigma^2} - \frac{|\underline{\mathbf{M}}|^2}{\chi^2} \right)}, \quad Z := \sigma^2(1 - \rho)e^{-\frac{|\underline{\mathbf{R}}|^2}{2\Sigma^2}} + \rho\chi^2 g,$$

where $\underline{\mathbf{R}}$ and Σ are defined in algorithm 2. These functions are not identical to the ones for the real case since in the prior distribution (3), the real and imaginary parts of the signal are jointly sparse (i.e. have same support but independent values), which can be a good assumption, for instance in MRI. As in c-LASSO [29], this allows to lower the phase transition compared to when the real and imaginary part of the signal are assumed to be independent.

The implementation requires caution: the necessary ‘‘structure killing’’ randomization is obtained by applying a permutation of lines after the use of the fast operator. For each block (r, c) , we choose a random subset of modes $\Omega^{r,c} = \{\Omega_1^{r,c}, \dots, \Omega_{N_r}^{r,c}\} \subset \{1, \dots, N_c\}$. The definition of $O_{\mu}(\mathbf{e}_c)$ using a standard fast transform FT will be:

$$O_{\mu}(\mathbf{e}_c) := \text{FT}(\mathbf{e}_c) \big|_{\Omega_{\mu - \mu_{r_{\mu}} + 1}^{r_{\mu}, c}} \quad (5)$$

where r_{μ} is the index of the block row that includes μ , $\mu_{r_{\mu}}$ is the number of the first line

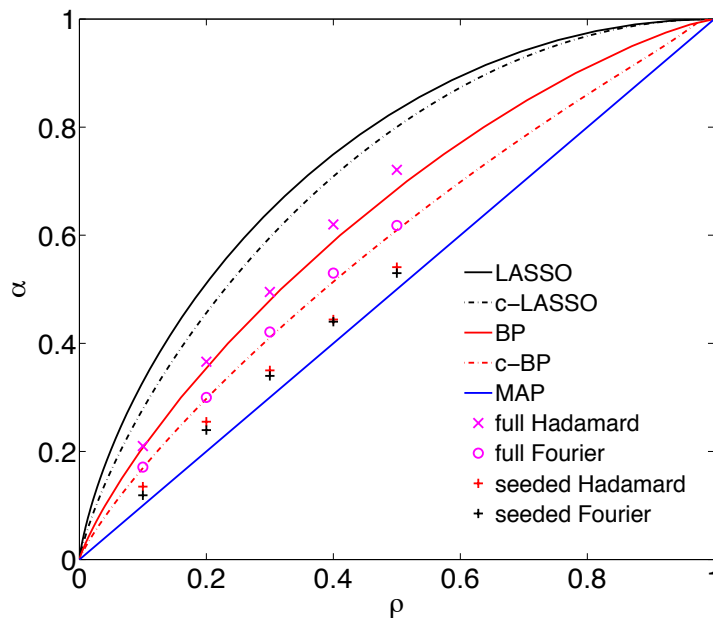


Figure 3. Phase diagram on the $\alpha = M/N$ (measurement rate) vs ρ (sparsity rate) plane in the noiseless case $\Delta = 0$. Lines are phase transitions predicted by the state evolution technique for i.i.d random Gaussian matrices, while markers are points from experiments using structured operators with empirically optimized parameters. Good sets of parameters usually lie in the following sets: ($L_c \in \{8, 16, 32, 64\}$, $L_r = L_c + \{1, 2\}$, $w \in \{2, \dots, 5\}$, $\sqrt{J} \in [0.2, 0.7]$, $\beta_{\text{seed}} \in [1.2, 2]$). With larger signals, higher values of L_c are better. Just as c-LASSO allows to improve the usual LASSO phase transition when the complex signal is sampled according to (3) (thanks to the joint sparsity of the real and imaginary parts), c-BP improves the usual BP transition. The line $\alpha = \rho$ is both the maximum-a-posteriori (MAP) threshold for CS and the (asymptotic) phase transition with spatially coupled matrices. Pink experimental points correspond to perfectly reconstructed instances using non spatially coupled Hadamard and Fourier operators (on the BP and c-BP phase transition respectively), the black and red points to spatially coupled ones (close to the MAP threshold). Properly randomized structured operators appear to have similar performances as random measurement matrices.

of the block row r_μ and $\lambda|_\mu$ is the μ^{th} component of λ . For $O_i^*(\mathbf{f}_r)$ instead,

$$O_i^*(\mathbf{f}_r) := \text{FT}^{-1}(\tilde{\mathbf{f}}_r) |_{i-i_{c_i}+1} \quad (6)$$

where c_i is the index of the block column that includes i , i_{c_i} is the number of the first column of the block column c_i , FT^{-1} is the standard fast inverse operator of FT and $\tilde{\mathbf{f}}_r$ is defined in the following way:

$$\forall \gamma \in \{1, \dots, N_r\}, \quad \tilde{\mathbf{f}}_r |_{\Omega_\gamma^{r,c}} = \mathbf{f}_r |_\gamma \quad \text{and} \quad \forall i \notin \Omega^{r,c}, \quad \tilde{\mathbf{f}}_r |_i = 0. \quad (7)$$

The mean squared error (MSE) achieved by the algorithm is:

$$E^t := \|\underline{\mathbf{a}}^t - \underline{\mathbf{x}}\|_2^2 = 1/N \sum_{i=1}^N |a_i^t - x_i|^2, \quad (8)$$

and measures how well the signal is reconstructed.

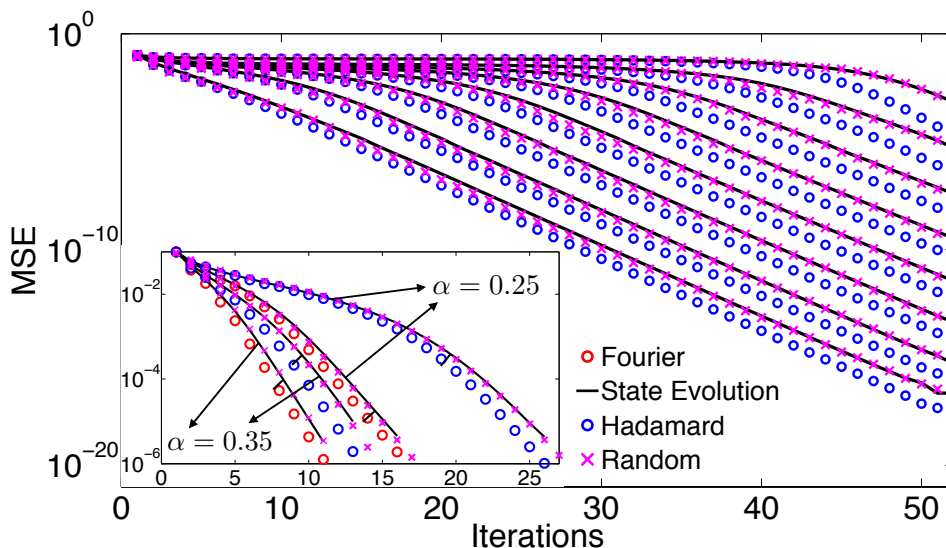


Figure 4. Comparison of the mean squared-error predictions between the SE (black lines) and the actual behavior of the algorithm for spatially coupled matrices (main figure) and standard ones (inset) both with structured operators (circles) and random i.i.d Gaussian matrices (crosses) in a noiseless compressed sensing problem. In both plots, the signal size is $N = 2^{14}$ with the random i.i.d Gaussian matrices, and $N = 2^{20}$ with the operators and are generated with $(\rho = 0.1, \bar{x} = 0, \sigma^2 = 1, \Delta = 0)$. While experiments made with random i.i.d matrices fit very well the SE predictions, those with the structured operators are not described well by the SE, although final performances are comparable. **Main:** For an Hadamard spatially coupled matrix as in Fig. 1 with $(L_c = 8, L_r = L_c + 2, w = 1, \sqrt{J} = 0.1, \alpha = 0.22, \beta_{\text{seed}} = 1.36)$. Each curve corresponds to the MSE tracked in a different block of the real signal \mathbf{x} (see Fig. 1). **Inset:** Reconstructions made with standard non spatially coupled (or full) matrices at $\alpha = 0.35$ and $\alpha = 0.25$. The reconstruction with the Fourier operator of a complex signal (instead of real with Hadamard) is faster thanks to the joint sparsity assumption of (3). The arrows identify the groups of curves corresponding to same measurement rate α . Both in the Fourier and Hadamard cases, we observe that convergence is slightly faster than predicted by the SE analysis.

2. Results for compressed sensing

When the sensing matrix is i.i.d random, or spatially coupled with i.i.d random blocks, the evolution of E^t in AMP can be predicted in the large signal limit on a rigorous basis called state evolution [19,27,31]. For BP with real Gauss-Bernoulli signals, this analysis can be found in [9]. For c-BP with i.i.d Gaussian matrices, the derivation goes very much along the same lines and we shall report the results briefly. The evolution of E^t is given by the following equation:

$$E^{t+1} = \int \mathcal{D}\underline{z} \left[(1 - \rho) f_{c_i} \left((\Sigma^t)^2, \underline{R}_1(\underline{z}) \right) + \rho f_{c_i} \left((\Sigma^t)^2, \underline{R}_2(\underline{z}) \right) \right], \quad (9)$$

where:

$$\underline{z} := z_1 + iz_2, \quad (\Sigma^t)^2 := (\Delta + E^t)/\alpha,$$

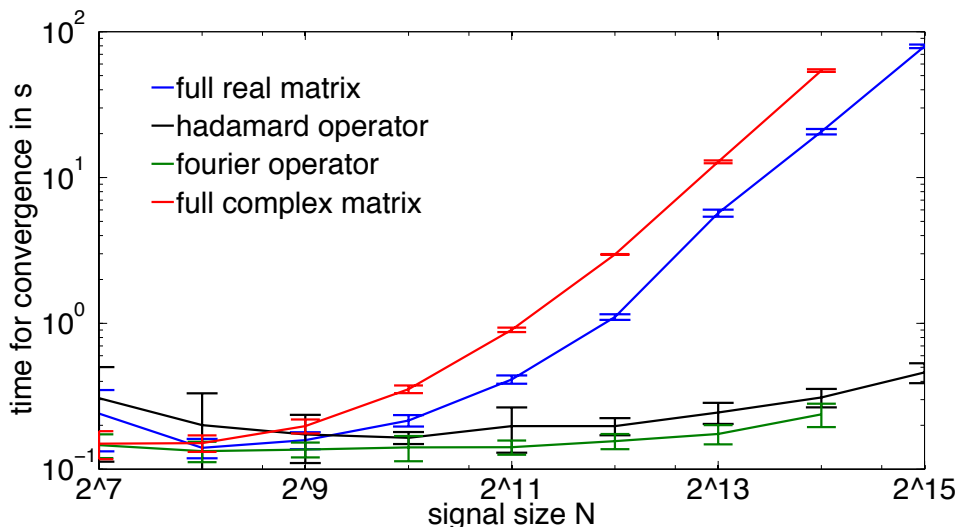


Figure 5. Time required for convergence (i.e. $\text{MSE} < 10^{-6}$) of the AMP algorithm in seconds as a function of the signal size, in the non spatially coupled case for a typical compressed sensing problem. The signal has distribution given by (3) and is real (complex) for the reconstruction with real (complex) matrices. The plot compares the speed of AMP with matrices (blue and red lines) to those of AMP using the structured operators (black and green lines). The points have been averaged over 10 random instances and the error bars represent the standard deviation with respect to these. The simulations have been performed on a personal laptop. As the signal size increases, the advantage of using operators becomes obvious.

$$\underline{R}_u^t(\underline{z}) := \underline{z} \sqrt{\sigma^2 \delta_{u,2} + (\Sigma^t)^2}, \quad \mathcal{D}_{\underline{z}} := dz_1 dz_2 \frac{e^{-\frac{1}{2}(z_1^2 + z_2^2)}}{2\pi}.$$

Note that this SE equation is the same as given in [29], despite slightly different update rules in the algorithm.

For c-BP with spatially coupled matrices with i.i.d Gaussian blocks, the expression involves the MSE in each block $p \in \{1, \dots, L_c\}$ (see main figure of Fig. 4), and becomes [9]:

$$E_p^{t+1} = \int \mathcal{D}_{\underline{z}} [(1 - \rho) f_c((\Sigma_p^t)^2, \underline{R}_{p,1}^t(\underline{z})) + \rho f_c((\Sigma_p^t)^2, \underline{R}_{p,2}^t(\underline{z}))],$$

where:

$$(\Sigma_p^t)^2 = \left[n_p \sum_{q=1}^{L_r} \frac{\alpha_q J_{qp}}{\Delta + \sum_{r=1}^{L_c} n_r J_{qr} E_r^t} \right]^{-1},$$

$$\underline{R}_{p,u}^t(\underline{z}) = \underline{z} \sqrt{\sigma^2 \delta_{u,2} + (\Sigma_p^t)^2},$$

where $n_i := N_i/N = 1/L_c$ for matrices with equally wide blocks (i.e. $N_i = N/L_c \forall i \in \{1, \dots, L_c\}$) as in Fig. 1, $\alpha_k = \alpha_{\text{rest}} + (\alpha_{\text{seed}} - \alpha_{\text{rest}}) \delta_{k,1}$ and J_{qp} is the variance of the elements belonging to the block at the q^{th} block row and p^{th} block column (1 or J in Fig. 1).

We now move to our main point. In the case of AMP with structured (Fourier or Hadamard) operators instead of i.i.d matrices, the SE analysis cannot be made. Hence

we experimentally compare the performances between AMP with structured operators and i.i.d matrices. The comparison is shown in Fig. 4, which opposes theoretical results from SE and experimental results obtained by running AMP on finite-sized data. On Fig. 3, we show the phase transition lines obtained by SE analysis in the (α, ρ) plane, and we added markers showing the position of instances actually recovered by the algorithm with spatially coupled structured operators in the noiseless case $\Delta = 0$.

2.1. Full operators

Let us first concentrate on AMP with non spatially coupled (or full) structured operators. The first observation is that the SE *does not* correctly describe the evolution of the MSE for AMP with full structured operators (inset Fig. 4). It is perhaps not surprising, given that AMP has been derived for i.i.d matrices. The difference is small, but clear: E^t decreases faster with structured operators than with i.i.d matrices. However, despite this slight difference in the dynamical behavior of the algorithm, the phase transitions and the final MSE performances for both approaches appear to be extremely close. As seen in Fig. 3, for small ρ , we cannot distinguish the actual phase transition with structured operators from the one predicted by SE. Thus, the SE analysis is still a good tool to predict the performances of AMP with structured operators.

2.2. Spatially coupled operators

For spatially coupled operators, the conclusions are similar (main plot on Fig. 4). Again, E_p^t (in each of the blocks of the signal induced by the spatially coupled structure of the measurement matrix) decreases faster with structured operators than with i.i.d matrices. But our empirical results are consistent (see Fig. 3) with the hypothesis that the proposed scheme, using spatially coupled Fourier/Hadamard operators, achieves correct reconstruction as soon as $\alpha > \rho$ when N is large. Indeed, we observe that the gap to the MAP threshold $\alpha_{\min} = \rho$ decreases as the signal size increases upon optimization of the spatially coupled operator structure. The results in Fig. 3 and Fig. 4 are obtained with spatially coupled matrices of the ensemble: $(L_c = 8, L_r = L_c + 1, w \in \{1, 2\}, \sqrt{J} \in [0.2, 0.5], \beta_{\text{seed}} = [1.2, 1.6])$. While these parameters do not quite saturate the bound $\alpha = \rho$ (which is only possible for $L_c \rightarrow \infty$ [8, 16, 19]), they do achieve near optimal performances. This, as well as the substantial cut in running time (Fig. 5) with respect to AMP with i.i.d matrices and the possibility to work with very large systems without saturating the memory, strongly supports the advantages of the proposed implementation of AMP.

3. Application to superposition codes

We shall now show how the present construction can be applied to a practical problem of coding theory: the sparse superposition codes introduced in [2, 24, 25] for error correction over the Gaussian channel. The AMP decoder for this problem has been studied in [26].

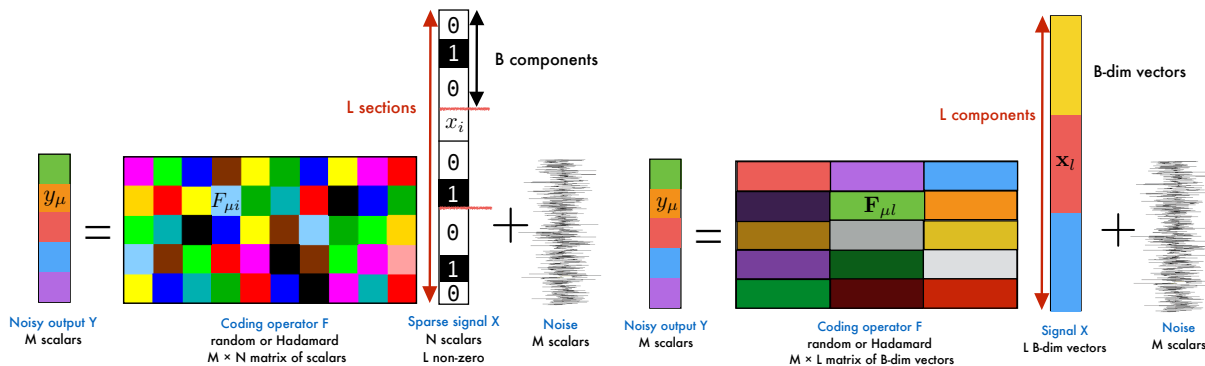


Figure 6. Left : Representation of the “compressed sensing like” problem associated to the decoding of the sparse signal over the AWGN channel, in terms of the usual 1-dimensional variables. In this setting, the variables in the same section $\{x_i : i \in l\}$ are strongly correlated due to the hard constraint that only one of them can be non-zero. The matrix elements are scalars as the signal components. **Right :** Re-interpretation of the decoding in terms of B -dimensional variables. In this version, the matrix elements are grouped to form B -dimensional vectors that are applied (using the usual scalar product for vectors) on the associated B -dimensional vectors representing the new components of the signal. The advantage of this setting is that now, the signal elements are uncorrelated, which is useful in the Bayesian setting to write a factorized prior distribution.

While these codes are capacity achieving [24], the AMP decoder is not [26] (at least without a proper power allocation). Our aim here is to show numerically that the spatially coupled Hadamard operator is appropriate to transmit close to the capacity, much in the same way spatial-coupling has been applied to Low Density Parity Check codes (LDPC) [32].

3.1. Superposition codes

Let us first give the basics of sparse superposition codes. Our goal is to transmit a real message $\tilde{\mathbf{x}} = \{\tilde{x}_i : i \in \{1, \dots, L\}, \tilde{x}_i \in \{1, \dots, B\} \forall i\}$ of size L through an Additive White Gaussian Noise (AWGN) channel, where a Gaussian noise with zero mean and variance Δ is independently added to all the components of the message that passes through it. $\tilde{\mathbf{x}}$ is first converted into \mathbf{x} which is made of L sections, each of size B : If the i^{th} component of the original message $\tilde{\mathbf{x}}$ is the k^{th} symbol of the alphabet, the i^{th} section of \mathbf{x} contains only zeros, except at the position k , where there is a positive value. Here, as in [26], we study the simplest setting, where the non-zero value in each section $l \in \{1, \dots, L\}$ is equal to 1. As an example, if $\tilde{\mathbf{x}} = [a, c, b, a]$ where the alphabet has only three symbols $\{a, b, c\}$ then \mathbf{x} made of 4 sections (one per symbol in the message $\tilde{\mathbf{x}}$) is $\mathbf{x} = [[100], [001], [010], [100]]$. \mathbf{x} is then encoded through a linear transform by application of the operator \mathbf{F} of size $M \times N$ and the resulting vector $\tilde{\mathbf{y}}$, the codeword, is sent through the Gaussian noisy channel which outputs a corrupted version \mathbf{y} to the receiver. The channel thus corresponds exactly to the model given by

(1), (2) with the same notations, and is represented in Fig. 7. The rate R denotes the number of informative bits sent per channel use. Defining $K := \log_2(B^L)$ as the number of informative bits in the signal \mathbf{x} made of L sections of size B ,

$$R := \frac{K}{M} = \frac{L \log_2(B)}{\alpha N} = \frac{\log_2(B)}{\alpha B}, \quad (10)$$

and therefore

$$M/N = \alpha = \log_2(B)/(RB) \rightarrow M = L \log_2(B)/R. \quad (11)$$

The capacity $C := 1/2 \log_2(1 + \text{snr})$ denotes the maximum rate achievable on the AWGN channel with power constrained codeword, where the signal to noise ratio is $\text{snr} := 1/\Delta$ (given the use of a proper rescaling of the matrix enforcing the power constraint $\|\tilde{\mathbf{y}}\|_2^2 = 1$). The capacity is independent of the coding and decoding scheme. We also define the optimal threshold as the best achievable rate using the present superposition coding strategy with a given section size B over the power constrained AWGN channel. This threshold actually tends to the capacity as B increases [26], see Fig. 10. Finally, the BP threshold is the rate until which the AMP decoder performs well combined with sparse superposition coding without the need of spatial coupling (such that it is optimal in the sense that the optimal threshold is the unique fixed point of the message passing equations). In the previous part on compressed sensing, the BP threshold was already present but as we were focusing on noiseless problems, the equivalent of the optimal threshold was identical to the MAP threshold which is the equivalent of the capacity here. In this framework, the error estimate we are interested in is the Section Error Rate (SER) which is the fraction of wrongly decoded sections:

$$\text{SER} := \frac{1}{L} \sum_{l=1}^L \mathbb{I}(\hat{x}_l \neq \tilde{x}_l), \quad (12)$$

where \hat{x}_l is the final estimate by the AMP algorithm of the l^{th} section, $l \in \{1, \dots, L\}$.

3.2. AMP decoding

Superposition codes are interesting in the present framework because the decoding task is actually equivalent to a multi-dimensional sparse-estimation problem [26]. As shown in Fig. 6, by considering the B -dimensional sections as the new variables, the linear system becomes the one considered in the compressed sensing setting. The prior $P(\mathbf{x})$ however is not (3), but instead imposes that each B -dimensional vector should have exactly one component equal to one and all the others equal to zero. In other words, the vector should point exactly toward one of the corners of the hyper-cube in B dimensions.

The AMP decoder for superposition codes [26] is thus equivalent to the one described in Fig. 2 with the only difference that the thresholding functions f_{a_i} and f_{c_i} are now functions of the sets $(\Sigma_l^{t+1}, \mathbf{R}_l^{t+1}) := \{(\Sigma_i^{t+1}, R_i^{t+1}) : i \in l\}$. Again, $i \in l$

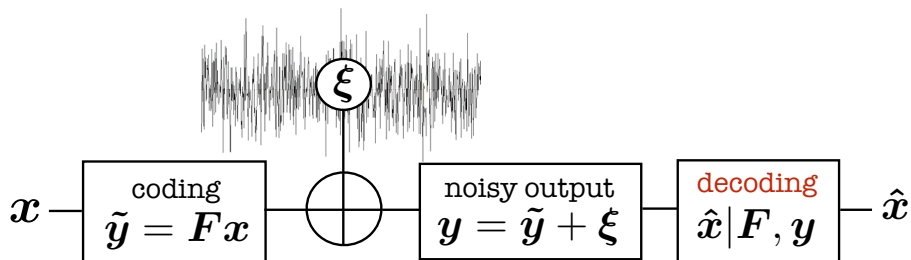


Figure 7. AWGN channel model: the message \mathbf{x} is coded by a linear transform, $\tilde{\mathbf{y}} = \mathbf{F}\mathbf{x}$ and then the real encoded message $\tilde{\mathbf{y}}$ is sent through the AWGN channel that adds an i.i.d Gaussian noise $\boldsymbol{\xi}$ with zero mean and a given variance Δ . The receptor gets the corrupted message \mathbf{y} and outputs an estimate $\hat{\mathbf{x}}$ of \mathbf{x} , knowing \mathbf{F} and \mathbf{y} . Perfect decoding means that $\hat{\mathbf{x}} = \mathbf{x}$.

means that x_i is a component of the l^{th} section of \mathbf{x} . These functions [26] are given by:

$$a_i^t := f_{a_i}(\boldsymbol{\Sigma}_l^{t+1}, \mathbf{R}_l^{t+1}) = \frac{e^{-\frac{1-2R_i^t}{2(\Sigma_i^t)^2}}}{\sum_{\{j \in l\}}^B e^{-\frac{1-2R_j^t}{2(\Sigma_j^t)^2}}}, \quad (13)$$

$$v_i^t := f_{c_i}(\boldsymbol{\Sigma}_l^{t+1}, \mathbf{R}_l^{t+1}) = a_i^t(1 - a_i^t). \quad (14)$$

The constraint imposed by $P(\mathbf{x})$ is much stronger than the one in compressed sensing, as it enforces binary values on the signal components and couples B of them. For this reason, perfect reconstruction might be possible even in a noisy setting. As for compressed sensing, the asymptotic performance of AMP for reconstruction in superposition codes is amenable to an analytic formula [26] using the state evolution technique. As for real and complex variables, state evolution for multi-dimensional variables can be demonstrated rigorously [33]. The analysis of AMP for i.i.d random matrices in the context of superposition codes has been performed using the state evolution technique in [26]. We have repeated this analysis for spatially coupled matrices and observed that, perhaps not surprisingly, one could asymptotically reach capacity (see Fig. 10). The object of the next section is thus to analyze the behavior of AMP when the i.i.d random matrices are replaced by full or spatially coupled structured operators as we did for compressed sensing.

3.3. Experimental results

A first observation is that performances very quickly converge to the ones with i.i.d random matrices with increasing alphabet size B . As in CS (see section 2), performances are thus asymptotically comparable. Fig. 8 shows the distance in dB from the BP threshold where the AMP decoder starts to get good reconstruction with i.i.d or structured matrices, as a function of B . It shows that structured operators reach quickly the i.i.d performances as B increases.

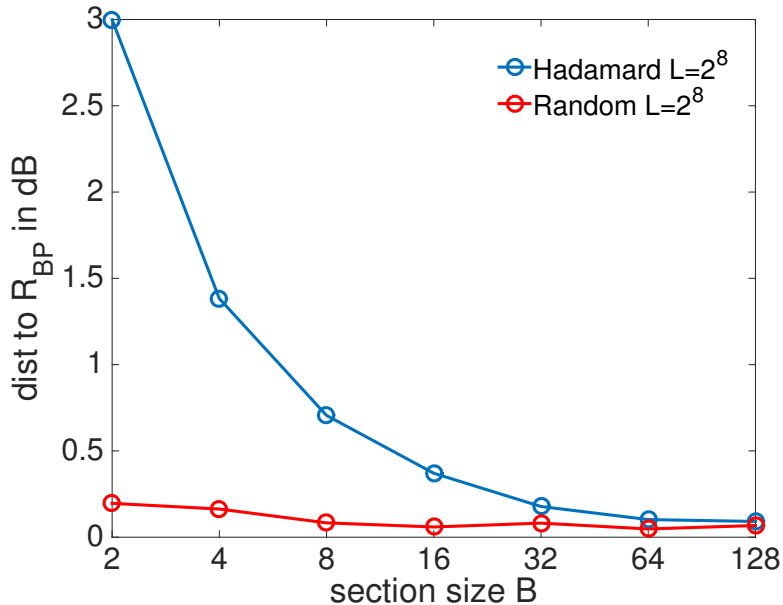


Figure 8. Comparison between the distance in dB to the asymptotic BP threshold R_{BP} at which the AMP decoder with full Hadamard structured coding operators (blue line) or with random i.i.d Gaussian matrices (red line) starts to reach an $SER < 10^{-5}$ (which is then almost always strictly 0) for a fixed number of sections $L = 2^8$ and $snr = 100$. The points have been obtained by averaging over 100 random instances. The BP threshold is obtained by state evolution analysis. The Hadamard operator works poorly when the signal density increases (i.e. when B decreases), but gets quickly closer to the random matrix performances as it decreases. The random Gaussian i.i.d matrices have a performance that is close to constant as a function of B , as it should at fixed L .

We now turn to the behavior of spatially coupled Hadamard operators by looking at the block error rate for different settings. The block error rate is the empirical probability of not perfectly reconstructing the signal (i.e. such that the final $SER > 0$). Fig. 9 shows how the finite size decreases the performance of the spatially coupled AMP reconstruction. For the purpose of numerical analysis, we used ($L_c = 16, L_r = L_c + 1, w = 2, \sqrt{J} = 0.4, \beta_{seed} = 1.8$) and considered two different values $snr = 15$ and $snr = 100$. For $B = 256$, the gain upon the standard AMP approach with full operators is consequent, even at these finite sizes. In all the experimental settings except ($snr = 15, B = 4$), the block error rate decreases as L increases, but in the high noise one with small section size ($snr = 15, B = 4$) the error is dominated by the noise influence and the finite size sensitivity is negligible despite that the SER effectively decreases as L increases. We observe that in the large section size $B = 256$ cases, the decoder performs well at rates larger than the BP threshold as expected. When B is small, the gap between the BP and optimal thresholds is too small to allow real improvement, but this gap gets larger as B and the snr increase. In addition, we see that the gap between the optimal threshold and the capacity decreases as B increases: superposition codes combined with spatially coupled operators are asymptotically capacity achieving [26] as

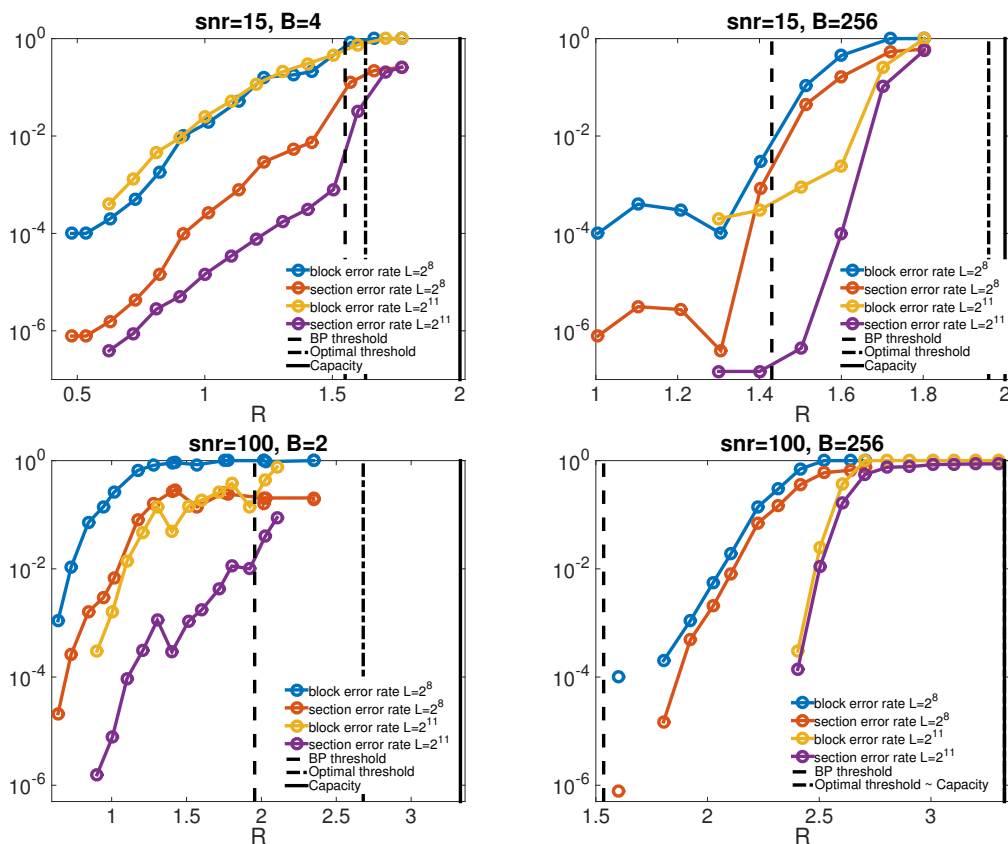


Figure 9. On this plot, we show the block error and section error rates of the superposition codes using AMP combined with the spatially coupled Hadamard operator for two different snr, two signal sizes L and two section sizes B . The block error rate is the fraction of the 10^4 random instances we ran for each point that have not been perfectly reconstructed, i.e. in these instances at least one section has not been well reconstructed (the final SER > 0). The section error rate is the fraction of wrongly decoded sections (12). The convergence criterion is that the mean change in the variables estimates between two consecutive iterations $\delta_{\max} < 10^{-8}$ and the maximum number of iterations is $t_{\max} = 3000$. The upper plots are for $\text{snr} = 15$, the lower for $\text{snr} = 100$ (notice the different x axes). The first dashed black line is the BP threshold obtained by state evolution analysis and marks the limit of efficiency of AMP *without* spatial coupling for large signals, the second one is the Bayes optimal threshold obtained by the replica method which is the best performance any decoder can reach with superposition codes for a given section size B (obtained by the replica method, the details can be found in [26]) and the solid black line is the capacity which bounds the performance of any coding scheme for this snr. In the ($\text{snr} = 100, B = 256$) case, the optimal threshold is so close to the capacity that we plot a single line. For such sizes, the block error rate is 0 for rates lower than the lowest represented rate. For $B = 256$, the sharp phase transition between the phases where reconstruction is possible/impossible by AMP with spatial coupling is clear. The spatially coupled operators used for the experiment are taken with parameters ($L_c = 16, L_r = L_c + 1, w = 2, \sqrt{J} = 0.4, \beta_{\text{seed}} = 1.8$), optimized heuristically.

$B \rightarrow \infty$. At large enough distance from C , the final SER is exactly zero in most of the cases, giving a low block error rate. This is due to the fact that in order to observe an $\text{SER} = O(\epsilon)$, there must be at least $L = O(1/\epsilon)$ sections, which is not the case for small signals, when the asymptotic SER is small. The optimal threshold is obtained by the replica method [26].

Fig. 10 shows the phase diagram for superposition codes at fixed $\text{snr} = 15$ for the same experiments as in [2]. The rate that can be reached is shown as a function of B . Comparing the black and yellow curves, it is clear that even without spatial coupling, AMP outperforms the iterative successive decoder of [2] for practical B 's. With the Hadamard spatially coupled AMP algorithm, this is true for any B and is even more pronounced (brown curve). The green (pink) curve shows that the full (spatially coupled) Hadamard operator has very good performances for reasonably large signals, corresponding here to a blocklength $M < 64000$ (the blocklength is the size of the transmitted vector $\tilde{\mathbf{y}}$).

4. Conclusion

We have presented a large empirical study using structured Fourier and Hadamard operators in sparse estimation problems. We have shown that combining these operators with a spatial coupling strategy allows to reach information-theoretical limits. We have tested our algorithm for noiseless compressed sensing, both for real and imaginary variables, and for the decoding of sparse superposition codes over the AWGN channel. With respect to [8, 9], the resulting algorithm is more efficient in terms of memory and running time. This allows us to deal with signal sizes as high as 10^6 and $\alpha \approx \rho$ on a personal laptop using MATLAB, and achieve perfect reconstruction in about a minute. We have released a Matlab implementation of our decoder at github.com/jeanbarbier/BPCS_common.

5. Acknowledgements

The research leading to these results has received funding from the European Research Council under the European Union's 7th Framework Programme (FP/2007-2013)/ERC Grant Agreement 307087-SPARCS and from the French Ministry of defense/DGA.

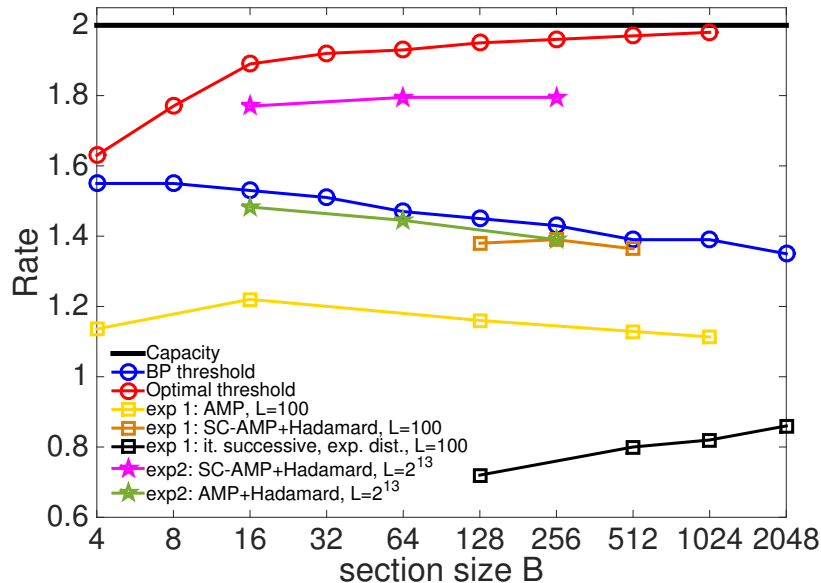


Figure 10. Phase diagram and experimental results for superposition codes: Numerical experiment at finite size L for $\text{snr} = 15$ and asymptotic results. The solid black line is the capacity, the blue line is the BP threshold obtained by state evolution analysis and the red line is the Bayesian optimal threshold (obtained by the replica method, the details can be found in [26]). The yellow, black and brown curves are results of the following experiment (exp 1): decode 10^4 random instances and identify the transition line between a phase where the probability p_ϵ to have a SER $> 10^{-1}$ is $p_\epsilon < 10^{-3}$ (below the line) from a phase where $p_\epsilon \geq 10^{-3}$ (more than 9 instances have failed over the 10^4 ones). The green and pink curves are the result of the second protocol (exp 2) which is a relaxed version of exp 1 with 10^2 random instances and $p_\epsilon < 10^{-1}$ (below the line), $p_\epsilon \geq 10^{-1}$ above. Note that in our experiments SER $< 10^{-1}$ essentially means SER = 0 at these sizes. The yellow curve compares our results with the iterative successive decoder (black curve) of [2, 24] where the number of sections $L = 100$. Note that these data, taken from [2, 24], have been generated with an exponential signal distribution rather than the $\{0, 1\}$ we used here. Compared with the yellow curve (AMP with the same value of L) the better quality of AMP reconstruction is clear. The green and pink curves are here to show the efficiency of the Hadamard operator with AMP with (pink curve) or without (green curve) spatial coupling. Comparing the brown and the pink curve shows the diminishing influence of finite size effects as L increases. The remaining gap between the pink curve and the optimal threshold is due to the still finite size of the signal. For the experimental results, the maximum number of iterations of the algorithm is arbitrarily fixed to $t_{max} = 500$. The parameters used for the spatially coupled operators are ($L_r = 16, L_c = L_r + 1, w = 2, \sqrt{J} = 0.3, \beta_s = 1.2$). Tuning these parameters could further improve performances.

- [1] D. L. Donoho, "Compressed sensing," *IEEE Trans. Inform. Theory*, vol. 52, pp. 1289, 2006.
- [2] A. R. Barron and A. Joseph, "Sparse superposition codes: Fast and reliable at rates approaching capacity with gaussian noise," *Manuscript. Available at <http://www.stat.yale.edu/~arb4>*, 2010.
- [3] E. Candès, J. Romberg, and T. Tao, "Robust uncertainty principles: Exact signal reconstruction

- from highly incomplete frequency information,” *IEEE Trans. Inform. Theory*, vol. 52, pp. 489–509, 2006.
- [4] M. F. Duarte, M. A. Davenport, D. Takhar, J. N. Laska, T. Sun, K. F. Kelly, and R. G. Baraniuk, “Single-pixel imaging via compressive sampling,” *Signal Processing Magazine, IEEE*, vol. 25, no. 2, pp. 83–91, 2008.
- [5] M. Mézard Zecchina R. and Parisi G., “Analytic and algorithmic solution of random satisfiability problems,” *Science*, vol. 297, no. 812, 2002.
- [6] M. Mézard and A. Montanari, *Information, physics, and computation*, Oxford University Press, 2009.
- [7] J. Barbier, F. Krzakala, L. Zdeborová, and P. Zhang, “The hard-core model on random graphs revisited,” in *Journal of Physics: Conference Series*. IOP Publishing, 2013, vol. 473, p. 012021.
- [8] F. Krzakala, M. Mézard, F. Sausset, Y.F. Sun, and L. Zdeborová, “Statistical physics-based reconstruction in compressed sensing,” *Phys. Rev. X*, vol. 2, pp. 021005, 2012.
- [9] F. Krzakala, M. Mézard, F. Sausset, Y.F. Sun, and L. Zdeborová, “Probabilistic reconstruction in compressed sensing: Algorithms, phase diagrams, and threshold achieving matrices,” *J. Stat. Mech.*, vol. P08009, 2012.
- [10] Y. Kabashima, F. Krzakala, M. Mézard, A. Sakata., and L. Zdeborová, “Phase transitions and sample complexity in bayes-optimal matrix factorization,” *CoRR*, vol. abs/1402.1298, 2014.
- [11] T. T. Do, T. D. Tran, and L. Gan, “Fast compressive sampling with structurally random matrices,” in *Acoustics, Speech and Signal Processing, 2008. ICASSP 2008. IEEE International Conference on*. IEEE, 2008, pp. 3369–3372.
- [12] D. L. Donoho, A. Maleki, and A. Montanari, “Message passing algorithms for compressed sensing: I. motivation and construction,” in *IEEE Information Theory Workshop (ITW)*, 2010, pp. 1–5.
- [13] D. L. Donoho, A. Maleki, and A. Montanari, “Message-passing algorithms for compressed sensing,” *Proc. Natl. Acad. Sci.*, vol. 106, no. 45, pp. 18914–18919, 2009.
- [14] S. Rangan, “Generalized approximate message passing for estimation with random linear mixing,” in *Proc. of the IEEE Int. Symp. on Inform. Theory (ISIT)*, 2011, pp. 2168–2172.
- [15] J. P. Vila and P. Schniter, “Expectation-maximization bernoulli-gaussian approximate message passing,” in *Proc. Asilomar Conf. on Signals, Systems, and Computers (Pacific Grove, CA)*, 2011.
- [16] S. Kudekar, T. Richardson, and R. Urbanke, “Threshold saturation via spatial coupling: Why convolutional ldpc ensembles perform so well over the bec,” in *Proc. of the IEEE Int. Symposium on Information Theory (ISIT)*, 2010, pp. 684–688.
- [17] S. Kudekar and H.D. Pfister, “The effect of spatial coupling on compressive sensing,” in *Communication, Control, and Computing (Allerton)*, 2010, pp. 347–353.
- [18] A. Yedla, Y. Jian, P.S. Nguyen, and H.D. Pfister, “A simple proof of threshold saturation for coupled scalar recursions,” arXiv:1204.5703v1 [cs.IT], 2012.
- [19] D.L. Donoho, A. Javanmard, and A. Montanari, “Information-theoretically optimal compressed sensing via spatial coupling and approximate message passing,” in *Proc. of the IEEE Int. Symposium on Information Theory (ISIT)*, 2012, pp. 1231–1235.
- [20] A. Javanmard and A. Montanari, “Subsampling at information theoretically optimal rates,” arXiv:1202.2525v1 [cs.IT], 2012.
- [21] U. S. Kamilov, A. Bourquard, and M. Unser, “Sparse image deconvolution with message passing,” SPARSE 2013.
- [22] M. Vehkaperä, Y. Kabashima, and S. Chatterjee, “Analysis of regularized ls reconstruction and random matrix ensembles in compressed sensing,” *arXiv preprint arXiv:1312.0256*, 2013.
- [23] C. Wen and K. Wong, “Analysis of compressed sensing with spatially-coupled orthogonal matrices,” *arXiv preprint arXiv:1402.3215*, 2014.
- [24] A. R. Barron and A. Joseph, “Analysis of fast sparse superposition codes,” in *Information Theory Proceedings (ISIT), 2011 IEEE International Symposium on*. IEEE, 2011, pp. 1772–1776.

- [25] A. R. Barron and S. Cho, “High-rate sparse superposition codes with iteratively optimal estimates,” in *Information Theory Proceedings (ISIT), 2012 IEEE International Symposium on*. IEEE, 2012, pp. 120–124.
- [26] J. Barbier and Krzakala F., “Replica analysis and approximate message passing decoder for superposition codes,” in *2014 IEEE International Symposium on Information Theory*, 2014.
- [27] M. Bayati and A. Montanari, “The dynamics of message passing on dense graphs, with applications to compressed sensing,” *IEEE Transactions on Information Theory*, vol. 57, no. 2, pp. 764–785, 2011.
- [28] P. Schniter and S. Rangan, “Compressive phase retrieval via generalized approximate message passing,” in *Communication, Control, and Computing (Allerton), 2012 50th Annual Allerton Conference on*. IEEE, 2012, pp. 815–822.
- [29] A. Maleki, L. Anitori, Z. Yang, and R. Baraniuk, “Asymptotic analysis of complex lasso via complex approximate message passing (camp),” 2012.
- [30] M. Mézard J. Barbier, F. Krzakala and L. Zdeborová, “Compressed sensing of approximately-sparse signals: Phase transitions and optimal reconstruction,” in *50th Annual Allerton Conference on Communication, Control, and Computing*, 2012.
- [31] M. Bayati, M. Lelarge, and A. Montanari, “Universality in polytope phase transitions and message passing algorithms,” *arXiv preprint arXiv:1207.7321*, 2012.
- [32] S. Kudekar, T. J. Richardson, and R. Urbanke, “Threshold saturation via spatial coupling: Why convolutional ldpc ensembles perform so well over the bec,” *Information Theory, IEEE Transactions on*, vol. 57, no. 2, pp. 803–834, 2011.
- [33] A. Javanmard and A. Montanari, “State evolution for general approximate message passing algorithms, with applications to spatial coupling,” *Information and Inference*, p. iat004, 2013.